의학박사 학위논문

췌장암 이종이식 모델에서 Doxorubicin을 탑재한 미세기포 집합체와 집속초음파 병행 치료의 상호증강 효과

Synergistic Effects of Pulsed Focused Ultrasound and a Doxorubicin-Loaded Microparticle–Microbubble Complex in a Pancreatic Cancer Xenograft Mouse Model

2021년 2월

서울대학교 의학대학원

의학과 영상의학전공

강 효 진

췌장암 이종이식 모델에서 Doxorubicin을 탑재한 미세기포 집합체와 집속초음파 병행 치료의 상호증강 효과

지도 교수 이 재 영

이 논문을 의학박사 학위논문으로 제출함
2021년 2월

서울대학교 대학원
의과대학 의학과
강 효 진

강효진의 의학박사 학위논문을 인준함
2021년 2월

위 원 장 김 태 유 (인)

부위원장 이 재 영 (인)

위 원 이 학 종

위 원 김 정 훈

위 원 이 은 선

Abstract

The synergistic effects of a doxorubicin (Dox)-loaded microparticle-microbubble complex (DMMC) and focused ultrasound (FUS) with a short duty cycle (5%) were evaluated in a pancreatic cancer xenograft model established by inoculating immunedeficient mice with CFPAC-1 cells. The efficacy of the DMMC with FUS (study 1), the effect of conjugating the particles as opposed to mixing them (study 2), and the levels of tumor apoptosis and intracellular Dox (study 3) were evaluated. The DMMC with FUS showed the lowest tumor growth rate (30.8 mm3/week) and the highest intracellular Dox uptake (8.8%) and tumor cell apoptosis rate (58.7%) among all treatments. The DMMC presented a significantly lower growth rate than the mixture of Dox-loaded microparticles and microbubbles (44.2 mm3/week, $P<0.01$) when they were combined with FUS. In conclusion, DMMC with short-duty-cycle FUS has promise for tumor growth suppression, which may be attributed to high intracellular Dox uptake.

Keywords : Pancreatic cancer; Xenograft; Focused ultrasound; Doxorubicin; Microbubbles

Student Number : 2016-36060

Table of Contents

List of Tables

List of Figures

List of Abbreviations

DMMC = doxorubicin-loaded microparticle-microbubble complex

DAPI = 4',6-diamidino-2-phenylindole

Dox = doxorubicin

DoxMP = doxorubicin-loaded microparticle

EM = electron microscopy

FBS = fetal bovine serum

FUS = focused ultrasound

MB = microbubble

PRF = pulse repetition frequency

TUNEL = terminal deoxynucleotidyl transferase-mediated dUTP nick end labeling

Introduction

Pancreatic cancer is the fourth most common cause of cancer-related death worldwide, and its incidence is still rising (1). Although complete (R0) resection in combination with systemic chemotherapy or chemoradiotherapy offers the only opportunity for a cure and relatively long-term survival (2), only a limited number of patients, approximately 20%, are suitable for margin-free resection surgery. The median survival of unresectable, locally advanced pancreatic cancer is 9-12 months, with proper chemotherapy or chemoradiotherapy.

As one of the promising concepts to overcome this medical challenge, augmenting drug delivery by physical stimulation, such as pH, redox, light, magnetic power or ultrasound energy, has flourished in recent years (3-8). Among these stimuli, pH and redox raise concerns regarding unwanted microenvironmental changes. Light stimulus seems to be safe but shows poor penetration; thus, it is only applicable to superficial targets. Magnetic power is only applicable with the use of paramagnetic particles. In contrast, ultrasound energy is safe, applicable to deep targets, and can be used without specific particles.

Focused ultrasound (FUS) is an emerging therapeutic modality that uses ultrasound waves to carry energy from an extracorporeal

source to the localized target area. Several studies have reported the efficacy and safety of FUS in various solid organs, such as the prostate, liver, bone, thyroid, and uterus (9–16). Depending on the FUS parameters, FUS can generate thermal and/or mechanical effects in targeted tissues. Thermal effects are predominantly observed under low spatial–average, temporal–average intensity (ISATA) levels with long exposure times, and mechanical effects are observed under high ISATA levels with short exposure times (13, 17, 18). The ISATA is determined by the acoustic pressure, pulse length, pulse repetition time/frequency, and total exposure time (18). Physiologically, thermal effects range from mild hyperthermia to thermal ablation and are related to energy absorption, and mechanical effects are related to acoustic cavitation, microstreaming, resultant shearing force, etc. (13). Hence, the final outcome of FUS is also affected by the characteristics of the target tissue, intervening tissue, or media (18).

According to recent studies, the mild thermal or mechanical effects of FUS may enhance drug delivery to the target (19–22). Particularly, pulsed FUS with a high intensity but a short duty cycle, which is prone to causing mechanical effects, enhances drug delivery to a greater extent without significant thermal damage to the targeted

tissue than pulsed FUS with a low intensity and a long duty cycle (21, 23, 24).

Many other methods to enhance drug delivery with ultrasound energy, such as the addition of microbubbles (MBs) or nano- or microparticles (MPs), have been investigated (25-29). Transient pore formation in the cell membrane (sonoporation) and the inertial cavitation of MBs generated by FUS can enhance drug delivery in an area not easily accessible by conventional methods (30). Moreover, MPs are often exploited as delivery vehicles via the encapsulation of therapeutic compounds that can cause systemic toxicity when delivered in their free form.

In this regard, the combination of well-known drug delivery augmentation methods-pulsed FUS, MBs and MPs-may maximize the drug delivery effect. Therefore, it can be hypothesized that an anticancer drug-loaded MP-MB complex combined with pulsed FUS at a short duty cycle has promise for effective cancer suppression. To investigate this hypothesis, the drug delivery effects of a doxorubicin (Dox)-loaded MP-MB complex (DMMC) with pulsed FUS were evaluated in a human pancreatic cancer xenograft mouse model in a sequence of in vivo studies.

Materials and Methods

This study was approved by the Institutional Animal Care and Use Committee of the Clinical Research Institute of Seoul National University Hospital.

Xenograft model of human pancreatic cancer

CFPAC-1 human pancreatic carcinoma cells (ATCC, Rockville, MD) were cultured in Dulbecco's modified Eagle's medium (DMEM, Invitrogen, San Diego, CA) supplemented with 10% fetal bovine serum (FBS, WelGene Co., Daejeon, Korea) and 1% penicillin (WelGene Co.) after digestion with 0.25% trypsin (WelGene Co.) at 37° C. A total of 5 × 106 cells suspended in 0.2 ml of media were subcutaneously injected into the right flank of 6-week-old BALB/c nude mice (Fig. 1a). For all in vivo animal experiments, general anesthesia was administered intraperitoneally using a mixture of zolazepam hydrochloride (30 mg/kg, Zoletil, Virbac, Seoul, Korea) and xylazine hydrochloride (10 mg/kg, Rompun 2%, Bayer Korea, Seoul, Korea). Tumors were allowed to grow for three weeks before the first treatment (Fig. 1b).

FUS system

A preclinical FUS system (VIFU2000®, Alpinion, Seoul, Korea)

was used throughout this study. The therapeutic transducer was composed of a single and spherical piezoelectric element with a 1.1 MHz resonance frequency. According to a previous study (23–25, 31, 32), pulsed FUS can enhance drug delivery significantly without significant thermal damage to the targeted tissue. Especially, Park et al. (23) reported that a higher mechanical index (MI) with a short duty cycle could enhance the chemotherapeutic effect to a greater extent than a lower MI with a long duty cycle at the same FUS energy level in a pancreatic cancer xenograft model. They have compared the chemotherapeutic effect of FUS with a duty cycle of 5% and 50% at the same energy level, and FUS with a 5% duty cycle presented a lower growth rate than with a 50% duty cycle. We adopted the parameters of FUS with a short duty cycle from the previous study for this study. The acoustic parameters used were as follows: peak–to–peak pressure, 24 MPa; peak–positive pressure, 14.8 MPa; peak–negative pressure, 9.2 MPa; –6 dB focal spot radius, 9.2 × 1.4 mm; acoustic power, 80.5 W; MI, 9.2; duty cycle, 5% (transmission time of a unit pulse, 1.25 ms; intermission time between pulses, 23.75 ms); pulse repetition frequency (PRF), 40 Hz; and total number of pulses, 800 (20 s). Since the procedure was performed with a 5% duty cycle and 40 Hz PRF, no

nonlinear effects were observed.

DMMC

Synthesis of Dox-albumin MPs (DoxMPs)

One gram of human serum albumin (HSA, Sigma-Aldrich, St. Louis, MO) was dissolved in 34 ml of deionized water, followed by the addition of 20 μl of 1 M NaOH solution. Then, 70 ml of anhydrous ethanol was slowly added over 5 min. After 30 min, 80 μl of 8% glutaraldehyde (Sigma-Aldrich) was added. Sixteen hours later, the solution was centrifuged at 18,000 rpm for 15 min. The supernatant was discarded, and the precipitate was dispersed in deionized water. Centrifugation and redispersion were repeated twice. Finally, the dispersed solution was centrifuged at 3,000 rpm for 5 min to remove the aggregates. Then, 5 ml of the albumin MP solution (100 mg) was added dropwise to 2 or 5 ml of the prepared Dox solution (2 mg/ml Dox solution, LC Laboratories, Woburn, MA) under stirring and protected from light. After 24 hours, the reaction solution was centrifuged at 18,000 rpm for 15 min. The supernatant was carefully collected for calculation of the encapsulation efficiency. The precipitate, the DoxMPs, was dissolved in deionized water. The encapsulation efficiency of Dox

from the supernatant was 98.6%, as determined by high-performance liquid chromatography (Agilent Technologies, 1260 Infinity II system, Santa Clara, CA) with a UV-visible detector. The size and zeta potential were characterized by dynamic light scattering (NanoZS90, Malvern, Worcestershire, UK).

Synthesis of microbubbles (MBs)

The MBs were synthesized by a phospholipid thin-film hydration method (33). 1,2-Distearoyl-sn-glycerol-3-phosphocholine (DSPC, NOF, Tokyo, Japan) and 1,2-distearoyl-sn-glycero-3-phosphoethanolamine-N-[succinyl(polyethylene--glycol)-2000] (DSPE-PEG2k-NHS, NOF) were dissolved in chloroform at a 9:1 molar ratio. The chloroform was evaporated to form a thin phospholipid film. This thin phospholipid film at a concentration of 0.5 mg/ml was hydrated using a 0.9% NaCl solution at the phase transition temperature of DSPC (55° C) in a bath sonicator. The headspace of the vial was filled with sulfur hexafluoride gas (SF6, Dong-A Scientific, Seoul, Korea). Sequentially, a hydrated liposomal precursor was activated using a mechanical vial agitator (Vialmix™, Lantheus Medical Imaging, North Billerica, MA) for 45 s to form MBs. The MBs were characterized by

dynamic light scattering (Malvern Zetasizer NanoZS90) and using a hemocytometer with an optical microscope (BX-43, Olympus, Tokyo, Japan). Serially diluted MB solutions were measured by dynamic light scattering to confirm the size of the MBs and using a hemocytometer to confirm the size and number of MBs.

Complexation of the DoxMPs and MBs (DMMC)

Two hundred microliters of the DoxMP solution was added into the as-prepared MB solution with pressure equalization. After gentle shaking or rocking for 0.5-1 hours, the DMMC was formed. The size and zeta potential were characterized by dynamic light scattering (NanoZS90, Malvern), an optical microscope (BX-43, Olympus) and a focused ion beam (Quanta™ 3D FEG, FEI Company, Eindhoven, the Netherlands). A schematic illustration and microscopic images of the DMMC and its proposed mechanism of action are presented in Fig. 2.

Experimental protocol

The in vivo experiment consisted of three studies: (i) study 1 was conducted to evaluate the efficacy of the DMMC with and without FUS compared to Dox with and without FUS; (ii) study 2 was conducted to evaluate the efficacy of the DMMC with FUS compared to a simple

mixture of Dox and MBs or DoxMPs and MBs with FUS; and (iii) study 3 was conducted to evaluate the histological features in all tested groups. The detailed experimental protocols are described in Table 1.

Study 1: Complex efficacy

Animals were divided into five groups (each group, n=5): 1) control; 2) Dox only; 3) Dox with FUS; 4) the DMMC only; and 5) the DMMC with FUS. Animals in all experimental groups were treated once per week for three weeks and were monitored for the following two weeks (a total of 4 weeks). Animals in all of the treated groups were administered Dox at a dose of 4 mg/kg (34) (200 μl of DMMC [80 μg/100 μl] or 40 μl of free Dox [2 mg/ml] per 20 g of each mouse). At the moment that the administration of Dox or the DMMC was started via the tail vein, the FUS treatment was started. The tumors were treated as much as possible at 2 mm intervals, and the number of treatments increased as the tumor grew. The tumor volume was measured every week during treatment and the post-treatment period. Measurements were performed by ultrasound for animals (E-Cube, Alpinion, Seoul, Korea) using an L3-12H linear probe (Fig. 3). The tumor volume was calculated with the following equation:

$$\text{Volume (mm3)} = \pi/6 \times \text{width (mm)} \times \text{length (mm)} \times \text{height (mm)}$$

Study 2: Efficacy of complex vs. mixture

Animals were divided into four groups (each group, n=5): 1) control; 2) Dox and MB mixture with FUS (Dox and MBs with FUS); 3) DoxMP and MB mixture with FUS (DoxMPs and MBs with FUS); and 4) the DMMC with FUS. Animals in all experimental groups were treated with a dose of 4 mg/kg Dox (34) (200 μl of DMMC [80 μg/100 μl] or 40 μl of free Dox [2 mg/ml] per 20 g of each mouse) once per week for three weeks and were monitored for the following four weeks (a total of 6 weeks). Under general anesthesia, the moment that the Dox, the drug mixture, or the DMMC started to be administered via the tail vein, FUS treatment started. The tumor was treated as much as possible, with a 2 mm interval, and the number of treatments was increased as the tumor grew. Tumor volumes were measured every week during the treatments and the post-treatment period.

Study 3: Histopathology

The animals were divided into seven groups, considering all possible combinations of Dox, DoxMPs, MBs, and/or FUS (each group,

n=3) for the histopathological study: 1) control; 2) Dox only; 3) Dox with FUS; 4) Dox and MBs with FUS; 5) DoxMPs and MBs with FUS; 6) the DMMC only; and 7) the DMMC with FUS. A dose of 4 mg/kg Dox (200 μl of DMMC [80 μg/100 μl] or 40 μl of free Dox [2 mg/ml] per 20 g of each mouse) was administered to animals in the treatment groups once per week for three weeks. Under general anesthesia, the moment that the Dox, the drug mixture, or the DMMC started to be administered via the tail vein, FUS treatment started. The tumors were treated as much as possible, with a 2mm interval, and the number of treatments was increased as the tumor grew. Immediately after the three treatments, the animals were euthanized, and the tumor tissues were excised. The obtained tumors were cryopreserved. Tissue sections (4 μm thick) were prepared using a microtome. Subsequently, the fluorescence-based quantity of Dox and the apoptosis ratio in the tumor tissue were assessed.

Fluorescence images of the tumor tissues were obtained using a LEICA TCS SP8 with an inverted microscope (DMI 600B, Leica Biosystems, Buffalo Grove, IL). Dox fluorescence was excited at 488 nm, and the emission was measured at 530 nm. Additionally, fluorescent 4′ ,6-diamidino-2-phenylindole (DAPI) staining was performed to

facilitate the identification of tumor cells. Post-imaging data analysis was performed using Aperio ImageScope software (version 12.3, Leica Biosystems) for three randomly selected regions of each tumor (nine regions per group). The ratio of Dox release in the tumor cells was calculated by the number of Dox fluorescence-emitting cells divided by the total cell number in the examined field.

Apoptotic cells were quantified by terminal deoxynucleotidyl transferase-mediated dUTP nick end-labeling (TUNEL) assay, which was performed using an ApopTag® peroxidase in situ apoptosis detection kit (S7100, Millipore, Billerica, MA). Additionally, methyl green staining was performed with TUNEL to facilitate the identification of apoptotic cells. The fraction of apoptotic cells in a tumor visualized under a high-power field (×200) was calculated by two researchers using ImageJ software (ImageJ, National Institutes of Health, Bethesda, MD) and Aperio ImageScope software (version 12.3, Leica Biosystems). Each researcher calculated the apoptotic cell fraction in five high-power fields, randomly and independently, producing ten values that were then averaged.

Statistical analysis

Continuous variables are expressed as the mean ± standard deviation. The mean tumor size, growth rate, Dox release and apoptotic cell count were analyzed using the Kruskal–Wallis test for multiple comparisons. For post hoc analysis, the Mann–Whitney test was used with Bonferroni's correction. Corrected P values less than 0.05 were considered to be statistically significant; thus, P values less than 0.01 for study 1 (5 groups), 0.013 for study 2 (4 groups) and 0.007 for study 3 (7 groups) were used as indicators of statistical significance. All statistical analyses were performed using commercially available software (SPSS version 23, IBM Corporation, Armonk, NY).

Results

Characterization of MPs, DoxMPs and the DMMC

The size and zeta potential of the albumin MPs were 156.1 ± 65.6 nm and −52.4 ± 8.1 mV, respectively; after Dox was coated onto the surface of the MPs, the physical properties were 169.3 ± 70.7 nm and −49.7 ± 7.4 mV, respectively. The MBs were 1.3 ± 0.3 μm in size and 1~5 × 109 per ml in concentration. After complexation, the size of the DMMC was 2.25 ± 0.7 μm, and the concentration was 0.2 ~ 1 x 109 per ml.

Study 1: Complex efficacy study

The mean tumor size at the first treatment (0 weeks) was 6.7 ± 1.4 mm3. The mean size of the tumor and their ranges per each group are tabulated in Table 2. The mean tumor volume in the DMMC with FUS group (66.14 ± 3.7 mm3) was significantly smaller than that in the Dox with FUS and control groups (100.36 ± 18.0 mm3, 130.10 ± 21.6 mm3, respectively) in the 4th week (P values < 0.05). A detailed time−tumor volume graph is shown in Fig. 4a. In particular, only the DMMC with FUS group presented a significantly slower tumor growth rate than the control group (14.4 ± 0.10 and 31.0 ± 5.5 mm3/week, respectively,

P=0.008) (Fig. 4b).

Study 2: Efficacy of complex vs. mixture

The mean tumor size at the first treatment (0 weeks) was 43.8 ± 11.9 mm3. The mean size of the tumor and their ranges per each group are tabulated in Table 2. The mean tumor volume in the DMMC with FUS group was the smallest among all tested groups at all follow-up points (Fig. 5a). Although the Dox and MB with FUS and DoxMP and MB with FUS groups presented lower growth rates than the control group, only the DMMC with FUS group presented a significantly slower growth rate than the control group (30.8 ± 1.4 and 56.2 ± 8.8 mm3/week, respectively, P=0.011) (Fig. 5b). In addition, the DMMC with FUS treatment presented a significantly slower tumor growth rate than the DoxMP and MB with FUS treatment (44.2 ± 2.7 mm3/week, P<0.01) (Fig. 5b).

Study 3: Histopathology

Significantly greater intratumoral Dox release was found in the DMMC with FUS group (8.8 ± 2.1% of tumor cells) than in the Dox only (0.77 ± 0.43%) and Dox with FUS (0.62 ± 0.22%) groups (P<0.001)

(Fig. 6a and 6b).

The mean tumor cell apoptosis rate in the DMMC with FUS group (58.7 ± 10.7%) was the highest among all tested groups and was significantly higher than that in the control group (13.8 ± 16.9%) (Fig. 7). In the representative images in Fig. 8, a massive area of complete tumor cell apoptosis appeared in the DMMC with the FUS group.

Table 1. Experimental protocol

	Purpose	Groups
Study 1	**Efficacy of Dox, FUS and DMMC** (n = 5 per group)	G1, No treatment (control) G2, Doxorubicin only (Dox only) G3, Doxorubicin with FUS (Dox with FUS) G4, Doxorubicin-loaded MP and MB complex (DMMC only) G5, DMMC with FUS (DMMC with FUS)
Study 2	**Efficacy of complex *vs.* mixture** (n = 5 per group)	G1, No treatment (control) G2, Doxorubicin and MB mixture with FUS (Dox and MB with FUS) G3, Doxorubicin-loaded MP and MB mixture with FUS (DoxMP and MB with FUS) G4, DMMC with FUS (DMMC with FUS)
Study 3	**Histopathology** (n = 3 per group)	G1, No treatment (control) G2, Doxorubicin only (Dox only) G3, Doxorubicin with FUS (Dox with FUS) G4, Doxorubicin and MB mixture with FUS (Dox and MB with FUS) G5, Doxorubicin-loaded MP and MB mixture with FUS (DoxMP and MB with FUS) G6, Doxorubicin-loaded MP and MB complex (DMMC only) G7, DMMC with FUS (DMMC with FUS)

Table 2. Mean tumor voulme at the first treatment (0 week)

	Groups	Mean ± SD (mm^3)	Range (mm3)
Study 1	Group 1	6.1 ± 0.3	4.8-6.8
	Group 2	6.5 ± 0.5	5.0-8.1
	Group 3	6.3 ± 0.6	4.5-8.1
	Group 4	6.7 ± 0.4	5.2-7.4
	Group 5	7.0 ± 0.9	4.9-10.8
	Average	6.7 ± 1.4	4.8-10.8
Study 2	Group 1	46.3 ± 2.8	39.8-46.3
	Group 2	45.5 ± 7.8	14.4-56.4
	Group 3	46.5 ± 2.4	38.0-51.2
	Group 4	44.6 ± 3.5	39.8-54.6
	Average	43.8 ± 11.9	14.4-56.4

SD = standard deviation

Figure 1. Gross pictures of mice (a) before inoculating CFPAC-1 and (b) after grown for three weeks (0 weeks).

(a)

(b)

Figure 2. Schematic and microscopic representation of doxorubicin-loaded microparticle-microbubble complex (DMMC) synthesis (not to scale) and the proposed mechanism of action of the DMMC.

(a) Doxorubicin-loaded microparticles (DoxMPs) were attached to the surface of the microbubbles (MBs) by an amide bond. The mean sizes of the DoxMPs and MBs are noted in the picture. (b) Microscopic images confirming DoxMP conjugation to the MBs. Electron microscopy (EM) image of DoxMPs (left upper) and optical transmission (right upper), fluorescent (left lower) and merged (right lower) images of the DMMC. Red fluorescence was emitted by Dox from the DoxMPs. The scale bar indicates 200 nm for the EM image and 10 μm for the other images. (c) When the DMMC is exposed to focused ultrasound (FUS), the DoxMPs dissociate from the DMMC. Simultaneously, FUS provokes inertial cavitation of the MBs with subsequent transient pore formation (sonoporation) in the cell membrane, which enhances DoxMP delivery into target cells. In addition, other DoxMPs are delivered to target cells by active cellular uptake.

(a)

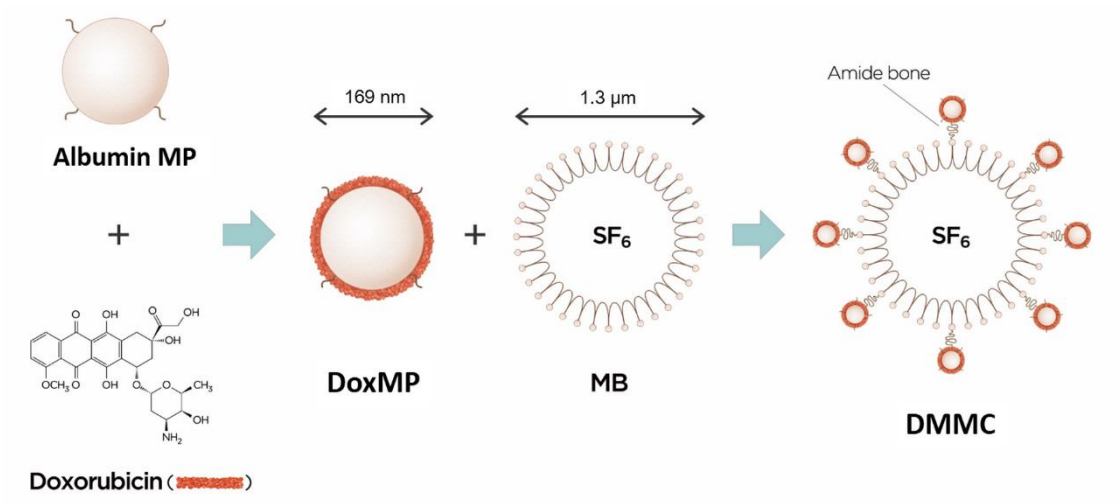
Albumin MP
+
Doxorubicin
169 nm
DoxMP
+
1.3 μm
SF6
MB
Amide bone
SF6
DMMC

(b)

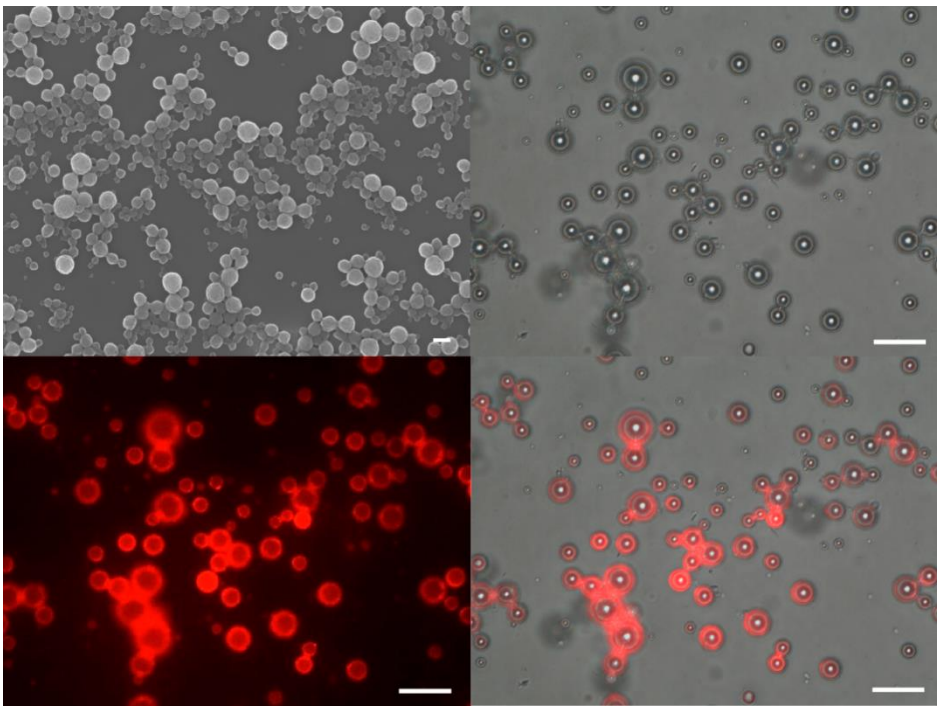

(c)

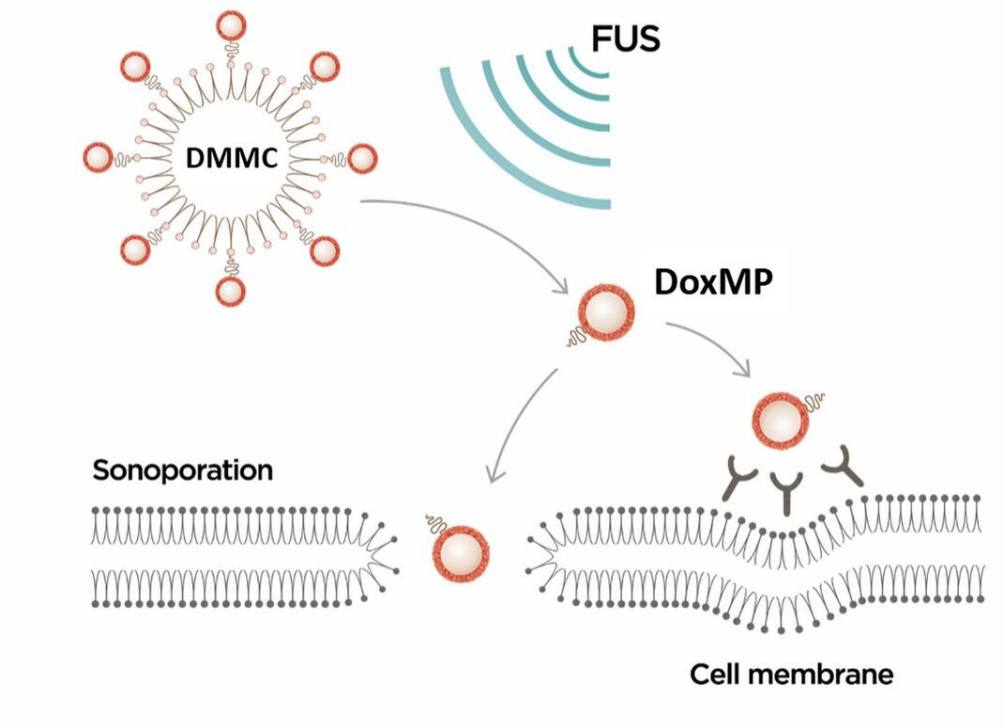

Figure 3. In vivo experimental setup and tumor size measurement by ultrasound. (a) The pancreatic cancer xenograft model was placed on a 3D positioning holder and submerged in 36° C degassed water. The FUS system had two transducers for treatment and imaging guidance. (b) The tumor volume was calculated by measuring the width, length and height of the tumor and applying the following equation: Volume (mm3) = π/6 × width (mm) × length (mm) × height (mm).

(a)

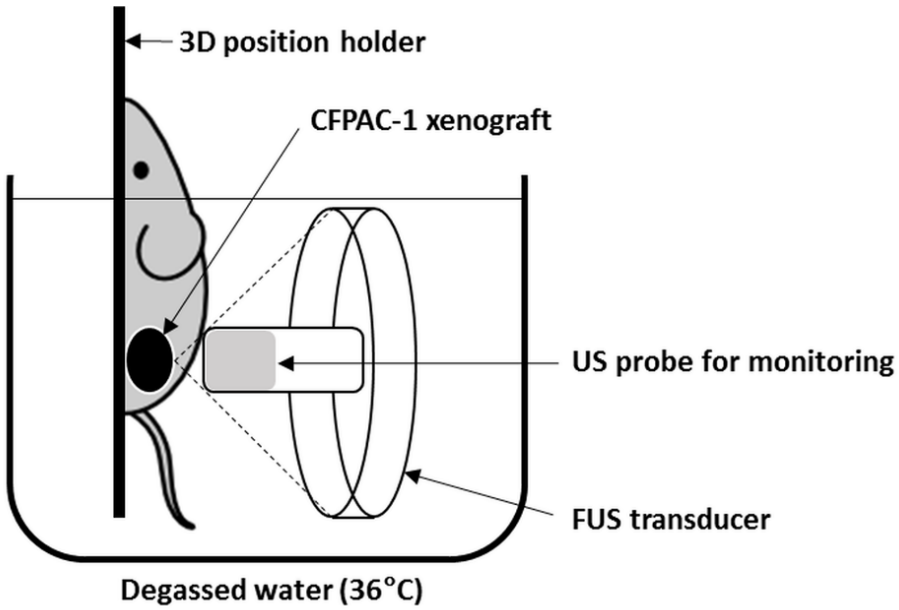
3D position holder
CFPAC-1 xenograft
US probe for monitoring
FUS transducer
Degassed water (36°C)

(b)

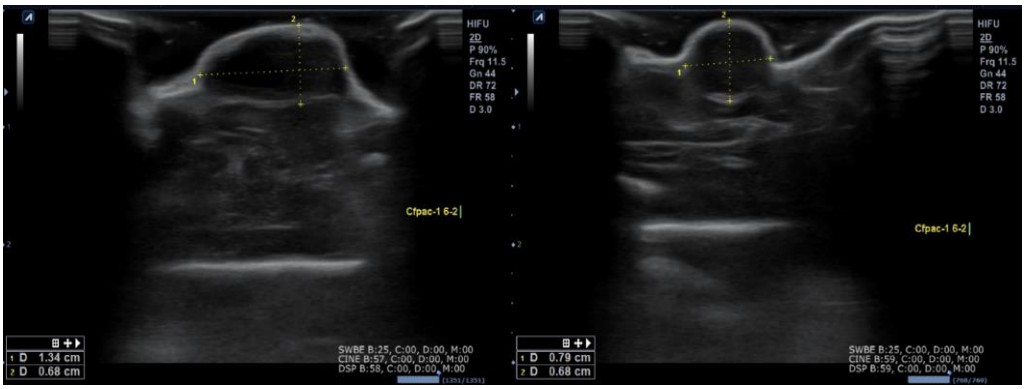
HIFU
2D
P 90%
Frq 11.5
Gn 44
DR 72
FR 58
D 3.0
Cfpac-1 6-2
D 1.34 cm
D 0.68 cm
D 0.79 cm
D 0.68 cm

Figure 4. Tumor volume and growth rate in study 1. (a) The DMMC with FUS group showed the smallest tumor size. (b) In the 4th week of the experiment, a significant difference in the tumor growth rate was found between the DMMC with FUS group (14.4 ± 0.1 mm3/week) and the control group (31.0 ± 5.5 mm3/week, P = 0.008). Empty arrows indicate treatments. FUS, focused ultrasound; Dox, doxorubicin; DMMC, doxorubicin-loaded microparticle-microbubble complex.

(a)

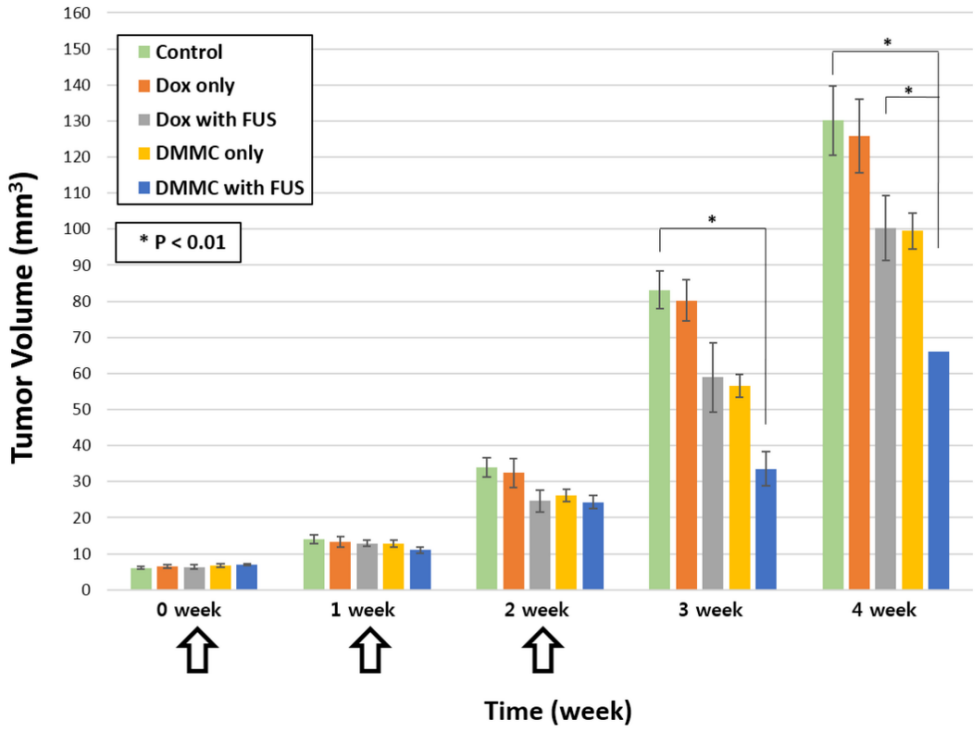
Tumor Volume (mm3)
160
150
140
130
120
110
100
90
80
70
60
50
40
30
20
10
0
Control
Dox only
Dox with FUS
DMMC only
DMMC with FUS
* P < 0.01
*
*
*
0 week
1 week
2 week
3 week
4 week
Time (week)

(b)

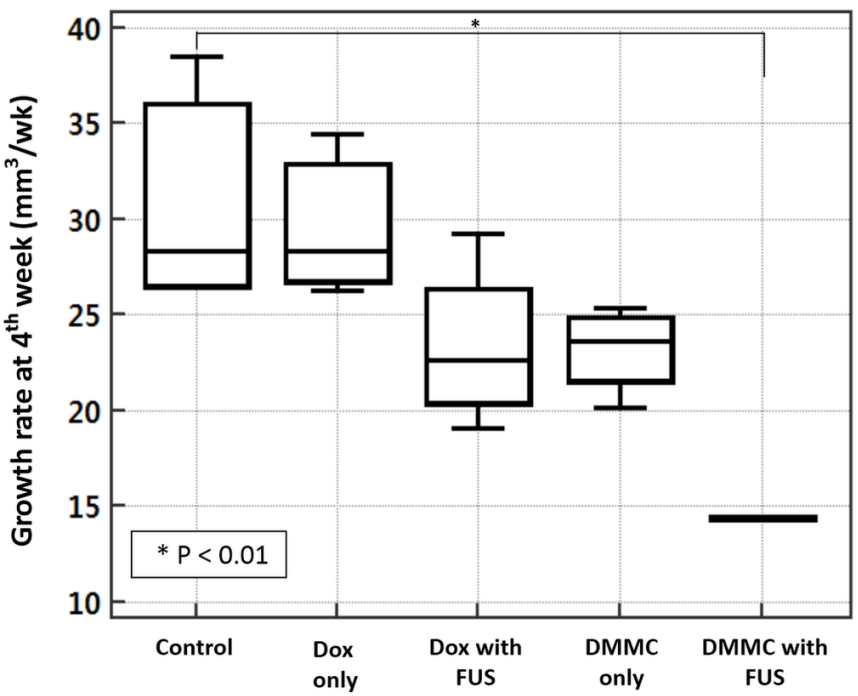
Growth rate at 4th week (mm3/wk)
40
35
30
25
20
15
10
*
* P < 0.01
Control
Dox only
Dox with FUS
DMMC only
DMMC with FUS

Figure 5. Tumor volume and growth rate in study 2. (a) The tumor volume in the DMMC with FUS group was the smallest throughout the entire follow-up period compared to that in the other groups. (b) The DMMC with FUS group (30.8 ± 1.4 mm3/week) was the only group showing a significantly lower value than that in the control group (56.2 ± 8.8 mm3/week, P = 0.011). Empty arrows indicate treatments. FUS, focused ultrasound; Dox, doxorubicin; MB, microbubble; DoxMP, doxorubicin-loaded microparticle; DMMC, doxorubicin-loaded microparticle-microbubble complex.

(a)

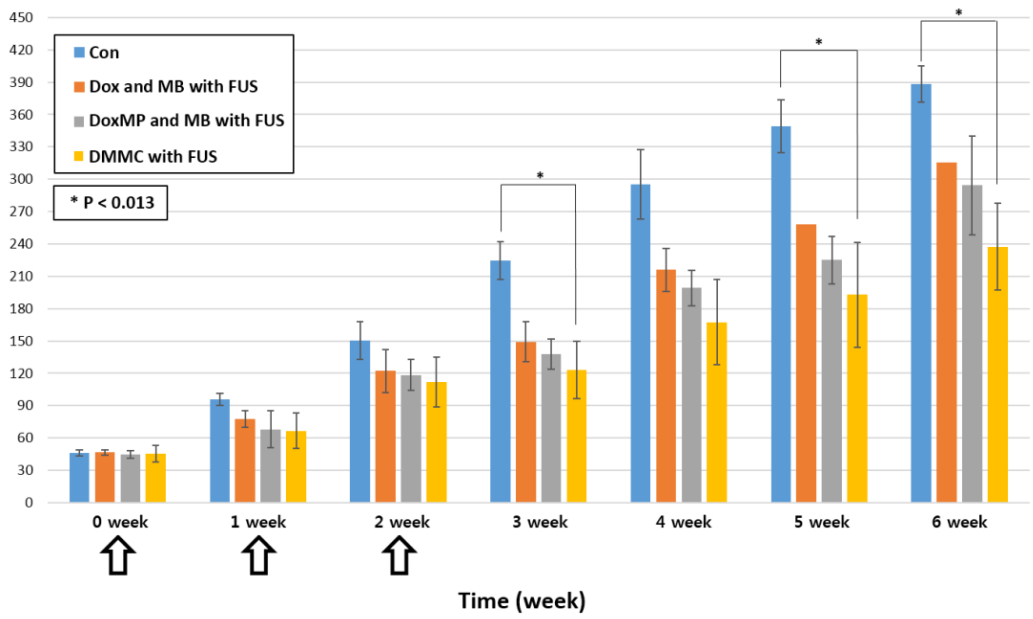
Con
Dox and MB with FUS
DoxMP and MB with FUS
DMMC with FUS
* P < 0.013
450
420
390
360
330
300
270
240
210
180
150
120
90
60
30
0
*
*
*
0 week
1 week
2 week
3 week
4 week
5 week
6 week
Time (week)

(b)

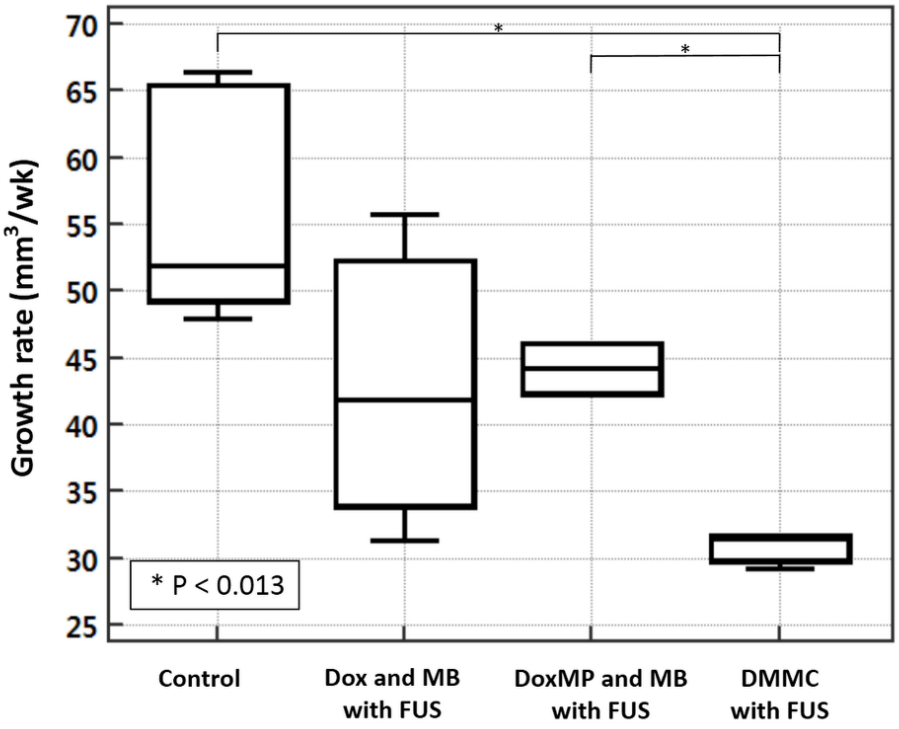
Growth rate (mm³/wk)
70
65
60
55
50
45
40
35
30
25
*
*
* P < 0.013
Control
Dox and MB with FUS
DoxMP and MB with FUS
DMMC with FUS

Figure 6. Quantification of Dox release in tumors and confocal microscopy images with DAPI staining in all experimental groups. (a) Significantly greater doxorubicin release was found in the DMMC with FUS group (8.8 ± 2.1% of tumor cells) than in the Dox only and Dox with FUS groups (P <0.001). (b) White represents DAPI-stained tumor cells, and red represents Dox. The multiple red dots in the DMMC with FUS group indicate released Dox. FUS, focused ultrasound; Dox, doxorubicin; MB, microbubble; DoxMP, doxorubicin-loaded microparticle; DMMC, doxorubicin-loaded microparticle-microbubble complex; DAPI, 4′,6-diamidino-2-phenylindole.

(a)

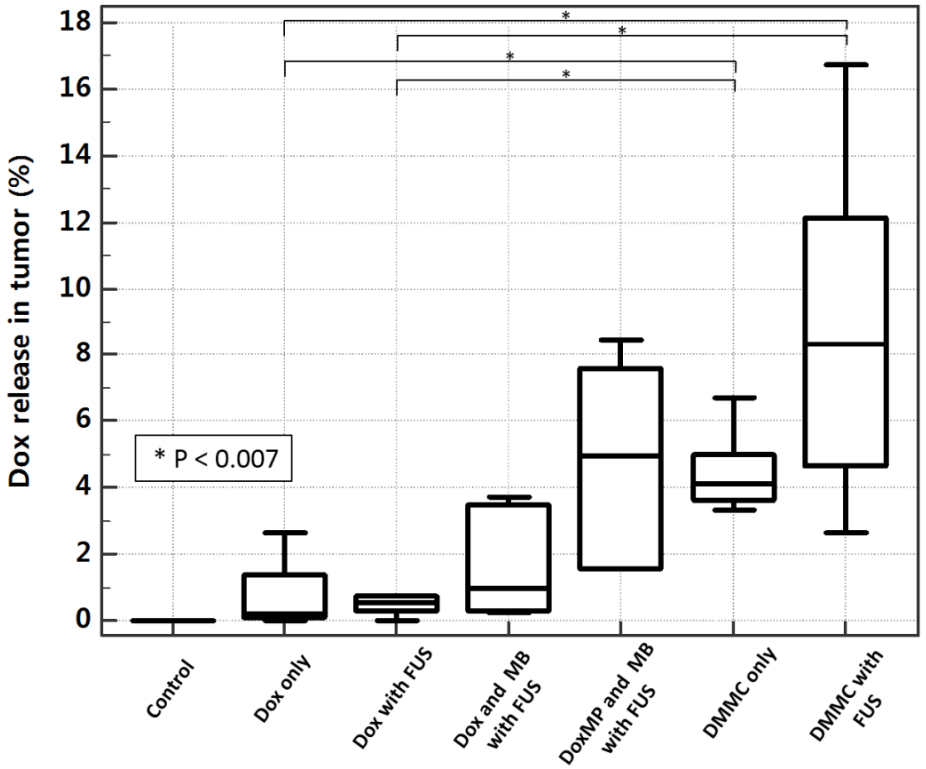
Dox release in tumor (%)
18
16
14
12
10
8
6
4
2
0
* P < 0.007
*
*
*
*
Control
Dox only
Dox with FUS
Dox and MB with FUS
DoxMP and MB with FUS
DMMC only
DMMC with FUS

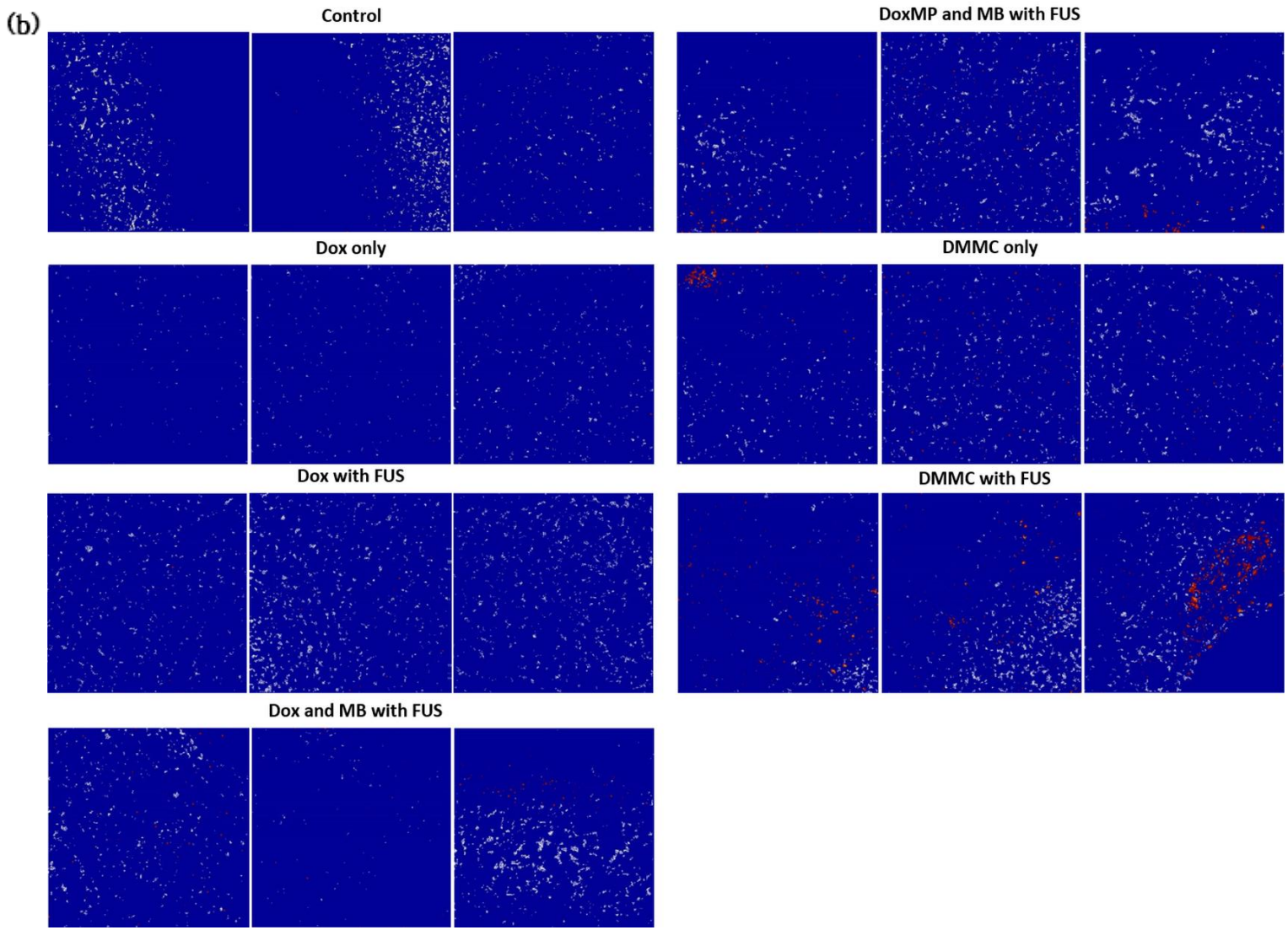
(b)
Control
DoxMP and MB with FUS
Dox only
DMMC only
Dox with FUS
DMMC with FUS
Dox and MB with FUS

Figure 7. The TUNEL assay showed a significantly higher apoptotic rate in the DMMC with FUS group than in the control group. FUS, focused ultrasound; Dox, doxorubicin; MB, microbubble; DoxMP, doxorubicin-loaded microparticle; DMMC, doxorubicin-loaded microparticle-microbubble complex.

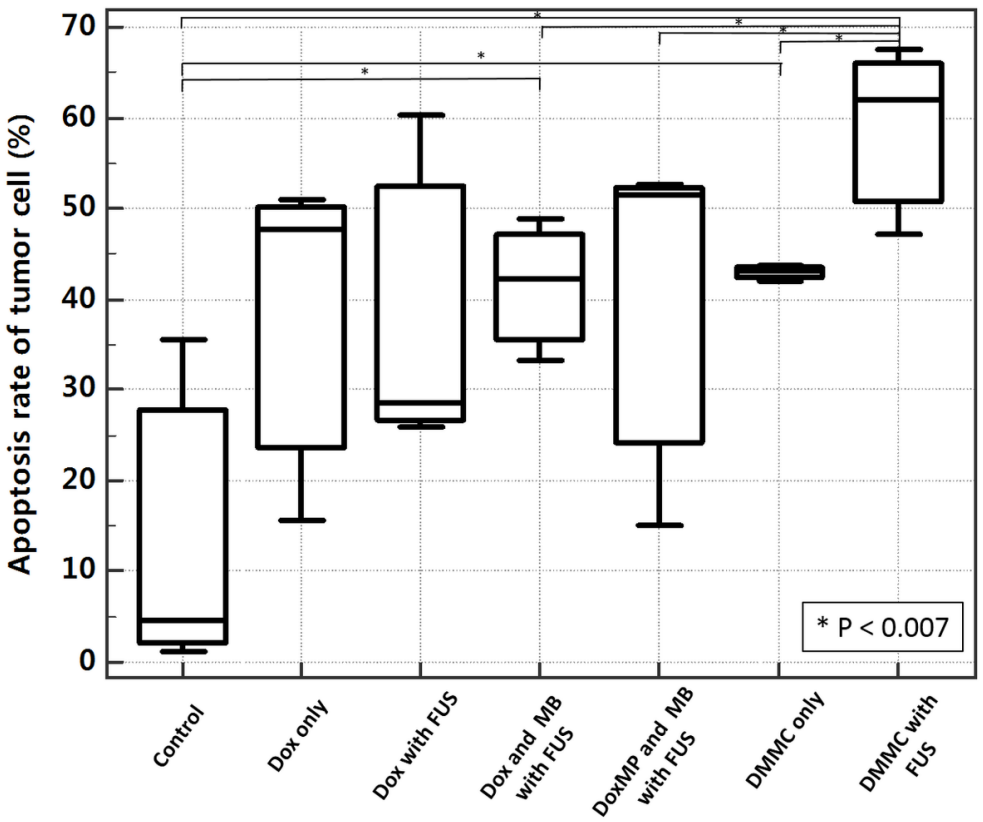

Figure 8. Representative images of the TUNEL assay with DAPI staining. Green represents the nucleus of the cell, and brown represents ongoing apoptosis. No apoptotic cells were detected in the control group (left upper). In the DoxMP and MB with FUS (right upper) and DMMC only (left lower) groups, partial necrosis was found in the tumor cells, while massive area of complete tumor cell necrosis were found in the DMMC with FUS group (right lower). FUS, focused ultrasound; Dox, doxorubicin; MB, microbubble; DoxMP, doxorubicin-loaded microparticle; DMMC, doxorubicin-loaded microparticle-microbubble complex.

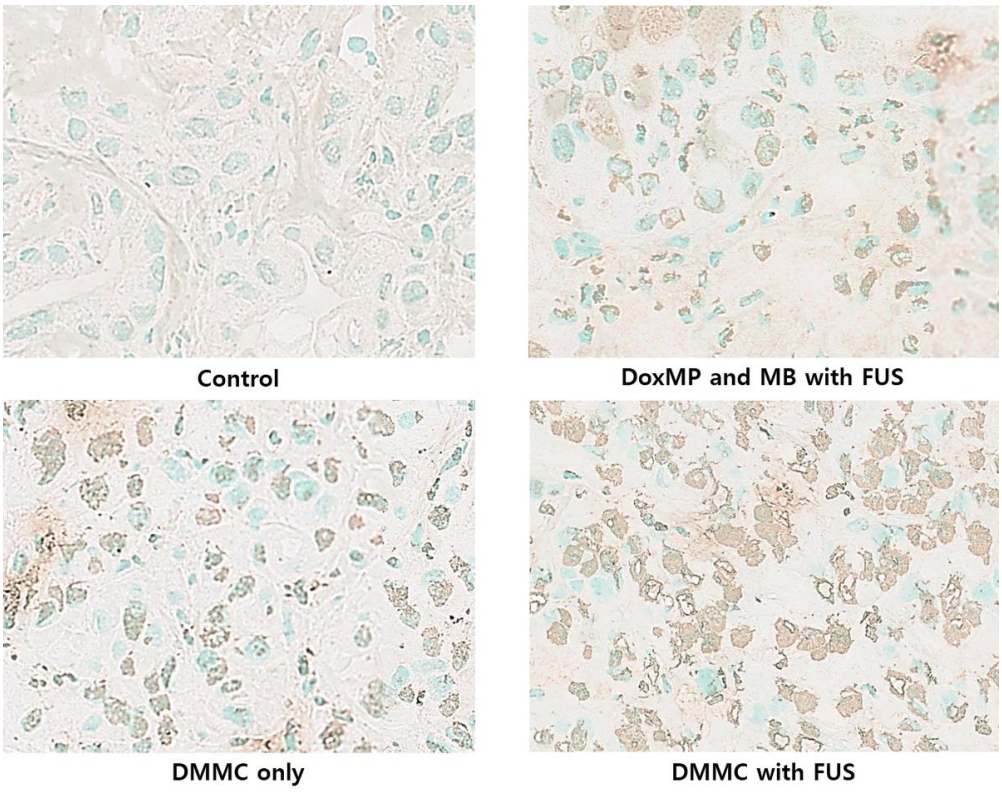

Discussion

In our study, we found that the DMMC with FUS showed the lowest tumor growth rate, the greatest Dox uptake in tumor cells, and the highest rate of tumor cell apoptosis among all the treatment groups (Figs. 6 and 7). The improved drug delivery and tumor suppressive effect of treatment with various particles and FUS compared with the control, Dox only, or DMMC only group was expected, as several previous studies have stated that pulsed FUS enhances drug delivery to target tissues by sonoporation (23, 25, 35). Interestingly, our study also shows that the DMMC formed by the complexation of DoxMPs and MBs resulted in a significantly slower growth rate than the mixture of DoxMPs and MBs when combined with FUS (Fig. 5b). These results may be explained by the following hypothesis: Complexation of the drug-containing MPs and MBs may play a role in effective drug delivery, as it prevents free extravasation to undesired tissue sites using the relatively large MBs (Fig. 2a). In addition, FUS may not only facilitate the selective release of drug-containing particles from the MBs but also allow these particles to penetrate cells efficiently by remodeling the extracellular matrix and increasing the

permeability of the cell membrane (19).

More specifically, most of the injected DMMCs are carried to a tumor without extravasation to undesired tissue sites. Upon arrival in the tumor, DoxMP dissociates from the MBs by FUS. Simultaneously, pulsed FUS provokes the inertial cavitation of MBs, which leads to increased extravasation of the drug by transient breaks in the endothelial cell lining of tumor vessels (36). DoxMPs then enter tumor cells with the increased cell membrane permeability achieved by the mechanical effects of FUS (37). This is consistent with a prior study by Lentacker et al. (37) on melanoma, which showed a two-fold higher anticancer effect using a Dox-liposome-loaded MB with therapeutic ultrasound compared with the Dox-liposome alone. Lin et al. reported that MB oscillation induced by FUS increased vascular permeability and led to greater nanoparticle deposition in tumors, as determined by immunoblotting analysis (38). Yu et al. revealed that MBs enhanced the anticancer effect of combined FUS and chemotherapy in a pancreatic cancer xenograft model (25).

In our study, the albumin MP was adopted as a Dox delivery vehicle. Interestingly, similar to the DMMC with FUS

group, the DoxMP and MB with FUS group presented significantly greater Dox release in tumor cells than the positive control group (Dox only), whereas the Dox and MB with FUS group did not (Fig. 6). The albumin shell, which allows active cellular uptake, may be mostly responsible for the greater ratio of Dox release in tumor cells.

Compared to other methods for augmenting drug delivery in pancreatic cancer, ultrasound-based stimulation is relatively safe and easily accessible. Thus, the FDA has approved the investigation of sonosensitive particles or materials investigated as anticancer drugs for combined chemosonodynamic therapy in pancreatic cancer. McEwan et al. proposed the use of oxygen-carrying MBs for the treatment of hypoxic tumors, such as those in pancreatic cancer (39). Nesbitt et al. investigated gemcitabine-functionalized oxygen-carrying MBs and revealed an effective anticancer effect in a pancreatic cancer xenograft model (40); however, these MBs carried the potential for oxygen radical toxicity.

In real practice, chemotherapy for pancreatic cancer is most effective when combined with chemotherapy agents (41-44). However, some patients were not able to endure the

systemic toxicity of combined chemotherapy. The reducing systemic toxicity of chemotherapy agents would enhance the tolerability as well as treatment efficacy. Our study used the Dox, one of the powerful cytotoxic agents, and possesses a successful anticancer effect (45). Dox has self-fluorescence (46) and albumin-friendly properties (47), which results in desirable conjugation with microparticles in our study. We have found that pulsed FUS may enhance drug delivery to pancreatic cancer cells, and further study with other chemotherapy agents such as gemcitabine is warranted.

Recently, the effect of microenvironmental changes by FUS have been reported by several studies (19, 48, 49). The tumor microenvironment comprised cancer cell, stromal cells, immune cells, vasculature, extracellular matrix, cytokine, chemokines and trophic factors (49). The microenvironmental change directly or indirectly influence tumor response. Among these, immunologic response by FUS attracted big attention. The mechanism and effect of immunologic response by FUS is not well established yet, but it seems to be a promising tool for cancer treatment. Indeed, the tumor growth are significantly related with immunologic environment. Inhibiting Hedgehog

signaling would enhance anti-cancer effect of chemotherapy (50). Activation of hypoxia-inducible factor 1α (HIF-1α) involved in the outgrowth and metastasis of cancer cell (51). Therefore, the immunologic analysis after FUS treatment with anticancer drugs, microbubbles and microparticles are very warranted.

In our study, we used a human pancreatic carcinoma cell line (CFPAC-1). It was inoculated at the right flank of 6-week-old BALB/C nude mice and grown for three weeks. Interestingly, CFPAC-1 (ATCC, Rockville, MD) in step 1 and 2 study presented different mean tumor size at three weeks after inoculation. This difference may be explained by the viability of the CFPAC-1 cell line. We have changed the preserved CFPAC-1 cell line between step 1 and 2 study, and this change makes a difference in the viability of the CFPAC-1 cell line. However, our study aims to compare the differences between groups in every step, not between study steps. Thus, the influence of these differences would be minimal.

Although our study successfully demonstrates the feasibility of FUS combined with the DMMC to enhance the anticancer effect in a xenograft model, several limitations need

to be acknowledged. First, we used fixed FUS conditions instead of investigating the most appropriate FUS parameters. However, we adopted the proper FUS conditions that were identified in a previous study at our institute (23). Second, the complexation of the DoxMPs and MBs may play a role in lowering the systemic toxicity compared with that in the other groups (DoxMP and MB, Dox and MB) when combined with FUS. However, we did not compare the systemic toxicity of the groups with the complex and mixture. Therefore, further studies are required to assess the toxicity of the complex compared with that of the mixture. Third, although the subcutaneous xenograft model is an established pancreatic cancer animal model, the pancreas is located deep in the abdomen and is surrounded by adjacent organs. Differences must exist in the penetration of ultrasound waves or disturbances caused by adjacent organs. Therefore, further studies are required for the optimization of the FUS parameters before clinical application. Fourth, although the TUNEL assay is sensitive and widely used to detect apoptosis, it could also label other cells with DNA damaged by necrosis or autolysis. Thus, the quantitative results of the TUNEL assay could be

overestimated. Fifth, although the quantitative analysis of intracellular Dox uptake by FACS is widely used for quantitative analysis, liquid chromatography would be a more accurate method for quantifying intracellular Dox level (52). However, the mean tumor size of our study was about 65 mm3 to 392 mm3, which was not enough to use liquid chromatography. Sixth, histopathologic analyses were not performed in steps 1 and 2 study. Although we performed step 3 study for histopathologic analysis by using seven groups of all possible combinations of Dox, DoxMPs, MBs, or FUS, the histopathologic analysis from the steps 1 and 2 study group would be more intuitive. In addition, the histopathologic analysis at the last week of experimentation would offer more information about the changes of the microenvironment, intracellular Dox uptake, and apoptosis. Last, the sample size is too small to generalize our results. However, as the very first study of the DMMC, the results could be used as a basis for a more extensive study.

Conclusion

Treatment with the DMMC and short-duty-cycle FUS has promise for tumor growth suppression, which may be attributed to high intracellular Dox uptake. This synergistic anticancer effect of the DMMC with FUS might be a promising approach for pancreatic cancer treatment.

References

1. Siegel RL, Miller KD, Jemal A. Cancer statistics, 2015. CA: a cancer journal for clinicians. 2015;65(1):5-29.
2. Hartwig W, Werner J, Jäger D, Debus J, Büchler MW. Improvement of surgical results for pancreatic cancer. The Lancet Oncology. 2013;14(11):e476-e85.
3. Sahle FF, Gulfam M, Lowe TL. Design strategies for physical-stimuli-responsive programmable nanotherapeutics. Drug discovery today. 2018;23(5):992-1006.
4. Liu J, Huang Y, Kumar A, Tan A, Jin S, Mozhi A, et al. pH-sensitive nano-systems for drug delivery in cancer therapy. Biotechnology advances. 2014;32(4):693-710.
5. McCarley RL. Redox-responsive delivery systems. Annual review of analytical chemistry. 2012;5:391-411.
6. Luo Z, Cai K, Hu Y, Li J, Ding X, Zhang B, et al. Redox-responsive molecular nanoreservoirs for controlled intracellular anticancer drug delivery based on magnetic nanoparticles. Advanced materials. 2012;24(3):431-5.
7. Rai P, Mallidi S, Zheng X, Rahmanzadeh R, Mir Y, Elrington S, et al. Development and applications of photo-triggered theranostic agents. Advanced drug delivery reviews. 2010;62(11):1094-124.
8. Stanley SA, Gagner JE, Damanpour S, Yoshida M, Dordick JS, Friedman JM. Radio-wave heating of iron oxide nanoparticles can regulate plasma glucose in mice.

Science. 2012;336(6081):604-8.
9. Lang BH, Woo YC, Wong CKH. High-Intensity Focused Ultrasound for Treatment of Symptomatic Benign Thyroid Nodules: A Prospective Study. Radiology. 2017;284(3):897-906.
10. Kim Y-s, Kim J-H, Rhim H, Lim HK, Keserci B, Bae D-S, et al. Volumetric MR-guided high-intensity focused ultrasound ablation with a one-layer strategy to treat large uterine fibroids: initial clinical outcomes. Radiology. 2012;263(2):600-9.
11. Poissonnier L, Chapelon J-Y, Rouviere O, Curiel L, Bouvier R, Martin X, et al. Control of prostate cancer by transrectal HIFU in 227 patients. European urology. 2007;51(2):381-7.
12. Illing R, Kennedy J, Wu F, Ter Haar G, Protheroe A, Friend P, et al. The safety and feasibility of extracorporeal high-intensity focused ultrasound (HIFU) for the treatment of liver and kidney tumours in a Western population. British journal of cancer. 2005;93(8):890-5.
13. Khokhlova TD, Hwang JH. HIFU for palliative treatment of pancreatic cancer. J Gastrointest Oncol. 2011;2(3):175-84.
14. Ghai S, Perlis N, Lindner U, Hlasny E, Haider MA, Finelli A, et al. Magnetic resonance guided focused high frequency ultrasound ablation for focal therapy in prostate cancer - phase 1 trial. Eur Radiol. 2018;28(10):4281-7.

15. Masciocchi C, Zugaro L, Arrigoni F, Gravina GL, Mariani S, La Marra A, et al. Radiofrequency ablation versus magnetic resonance guided focused ultrasound surgery for minimally invasive treatment of osteoid osteoma: a propensity score matching study. European radiology. 2016;26(8):2472-81.
16. Lang BH, Woo YC, Chiu KW. Role of second high-intensity focused ultrasound (HIFU) treatment for unsatisfactory benign thyroid nodules after first treatment. Eur Radiol. 2018:1-10.
17. Hoogenboom M, Eikelenboom D, den Brok MH, Heerschap A, Fütterer JJ, Adema GJ. Mechanical high-intensity focused ultrasound destruction of soft tissue: working mechanisms and physiologic effects. Ultrasound in medicine & biology. 2015;41(6):1500-17.
18. Ebbini ES, Ter Haar G. Ultrasound-guided therapeutic focused ultrasound: current status and future directions. International journal of hyperthermia. 2015;31(2):77-89.
19. Lee S, Han H, Koo H, Na JH, Yoon HY, Lee KE, et al. Extracellular matrix remodeling in vivo for enhancing tumor-targeting efficiency of nanoparticle drug carriers using the pulsed high intensity focused ultrasound. Journal of Controlled Release. 2017;263:68-78.
20. Farr N, Wang Y-N, D'Andrea S, Starr F, Partanen A, Gravelle KM, et al. Hyperthermia-enhanced targeted drug delivery using magnetic resonance-guided focussed ultrasound: a pre-clinical study in a genetic model of pancreatic cancer. International Journal of

Hyperthermia. 2017;34(3):284-91.

21. Lee ES, Lee JY, Kim H, Choi Y, Park J, Han JK, et al. Pulsed high-intensity focused ultrasound enhances apoptosis of pancreatic cancer xenograft with gemcitabine. Ultrasound in medicine & biology. 2013;39(11):1991-2000.

22. Bing C, Patel P, Staruch RM, Shaikh S, Nofiele J, Wodzak Staruch M, et al. Longer heating duration increases localized doxorubicin deposition and therapeutic index in Vx2 tumors using MR-HIFU mild hyperthermia and thermosensitive liposomal doxorubicin. International Journal of Hyperthermia. 2019;36(1):196-203.

23. Park EJ, Ahn YD, Lee JY. In vivo study of enhanced chemotherapy combined with ultrasound image-guided focused ultrasound (USgFUS) treatment for pancreatic cancer in a xenograft mouse model. Eur Radiol. 2018;28(9):3710-8.

24. Park M, Kim Y, Yang J, Sun W, Park H, Chae S, et al. Pulsed high-intensity focused ultrasound therapy enhances targeted delivery of cetuximab to colon cancer xenograft model in mice. Ultrasound in medicine & biology. 2013;39(2):292-9.

25. Yu MH, Lee JY, Kim HR, Kim BR, Park E-J, Kim HS, et al. Therapeutic Effects of Microbubbles Added to Combined High-Intensity Focused Ultrasound and Chemotherapy in a Pancreatic Cancer Xenograft Model. Korean journal of radiology. 2016;17(5):779-88.

26. Mullin LB, Phillips LC, Dayton PA. Nanoparticle delivery

enhancement with acoustically activated microbubbles. IEEE transactions on ultrasonics, ferroelectrics, and frequency control. 2013;60(1):65-77.

27. Halford A, Ohl C-D, Azarpazhooh A, Basrani B, Friedman S, Kishen A. Synergistic effect of microbubble emulsion and sonic or ultrasonic agitation on endodontic biofilm in vitro. Journal of endodontics. 2012;38(11):1530-4.

28. Mannaris C, Yang C, Carugo D, Owen J, Lee JY, Nwokeoha S, et al. Acoustically responsive polydopamine nanodroplets: A novel theranostic agent. Ultrasonics sonochemistry. 2020;60:104782.

29. Kwan JJ, Myers R, Coviello CM, Graham SM, Shah AR, Stride E, et al. Ultrasound-propelled nanocups for drug delivery. Small. 2015;11(39):5305-14.

30. Hancock HA, Smith LH, Cuesta J, Durrani AK, Angstadt M, Palmeri ML, et al. Investigations into pulsed high-intensity focused ultrasound–enhanced delivery: preliminary evidence for a novel mechanism. Ultrasound in medicine & biology. 2009;35(10):1722-36.

31. Timbie KF, Mead BP, Price RJ. Drug and gene delivery across the blood–brain barrier with focused ultrasound. Journal of Controlled Release. 2015;219:61-75.

32. Simoni V, Cafarelli A, Tognarelli S, Menciassi A, editors. Ex Vivo Assessment of Multiple Parameters in High Intensity Focused Ultrasound. 2018 40th Annual International Conference of the IEEE Engineering in Medicine and Biology Society (EMBC); 2018: IEEE.

33. Tinkov S, Coester C, Serba S, Geis NA, Katus HA, Winter G, et al. New doxorubicin-loaded phospholipid microbubbles for targeted tumor therapy: in-vivo characterization. Journal of Controlled Release. 2010;148(3):368-72.
34. Gabizon A, Shmeeda H, Barenholz Y. Pharmacokinetics of pegylated liposomal doxorubicin. Clinical pharmacokinetics. 2003;42(5):419-36.
35. Lee JY, Choi BI, Ryu JK, Kim Y-T, Hwang JH, Kim SH, et al. Concurrent chemotherapy and pulsed high-intensity focused ultrasound therapy for the treatment of unresectable pancreatic cancer: initial experiences. Korean journal of radiology. 2011;12(2):176-86.
36. Van Wamel A, Kooiman K, Harteveld M, Emmer M, Folkert J, Versluis M, et al. Vibrating microbubbles poking individual cells: drug transfer into cells via sonoporation. Journal of controlled release. 2006;112(2):149-55.
37. Lentacker I, Geers B, Demeester J, De Smedt SC, Sanders NN. Design and evaluation of doxorubicin-containing microbubbles for ultrasound-triggered doxorubicin delivery: cytotoxicity and mechanisms involved. Molecular Therapy. 2010;18(1):101-8.
38. Lin C-Y, Liu T-M, Chen C-Y, Huang Y-L, Huang W-K, Sun C-K, et al. Quantitative and qualitative investigation into the impact of focused ultrasound with microbubbles on the triggered release of nanoparticles from vasculature in mouse tumors. Journal of Controlled

Release. 2010;146(3):291-8.

39. McEwan C, Owen J, Stride E, Fowley C, Nesbitt H, Cochrane D, et al. Oxygen carrying microbubbles for enhanced sonodynamic therapy of hypoxic tumours. Journal of controlled release. 2015;203:51-6.

40. Nesbitt H, Sheng Y, Kamila S, Logan K, Thomas K, Callan B, et al. Gemcitabine loaded microbubbles for targeted chemo-sonodynamic therapy of pancreatic cancer. Journal of Controlled Release. 2018;279.

41. Yoo C, Hwang J, Kim J, Kim T, Lee J, Park D, et al. A randomised phase II study of modified FOLFIRI. 3 vs modified FOLFOX as second-line therapy in patients with gemcitabine-refractory advanced pancreatic cancer. British journal of cancer. 2009;101(10):1658-63.

42. Heinemann V, Haas M, Boeck S. Systemic treatment of advanced pancreatic cancer. Cancer treatment reviews. 2012;38(7):843-53.

43. Saung MT, Zheng L. Current standards of chemotherapy for pancreatic cancer. Clinical therapeutics. 2017;39(11):2125-34.

44. Neoptolemos JP, Kleeff J, Michl P, Costello E, Greenhalf W, Palmer DH. Therapeutic developments in pancreatic cancer: current and future perspectives. Nature reviews Gastroenterology & hepatology. 2018;15(6):333-48.

45. Shi Y, Moon M, Dawood S, McManus B, Liu P. Mechanisms and management of doxorubicin cardiotoxicity. Herz. 2011;36(4):296-305.

46. Shah S, Chandra A, Kaur A, Sabnis N, Lacko A,

Gryczynski Z, et al. Fluorescence properties of doxorubicin in PBS buffer and PVA films. Journal of Photochemistry and Photobiology B: Biology. 2017;170:65-9.

47. Yousefpour P, Ahn L, Tewksbury J, Saha S, Costa SA, Bellucci JJ, et al. Conjugate of Doxorubicin to Albumin-Binding Peptide Outperforms Aldoxorubicin. Small. 2019;15(12):1804452.

48. Eranki A, Srinivasan P, Ries M, Kim A, Lazarski CA, Rossi CT, et al. High-Intensity Focused Ultrasound (HIFU) Triggers Immune Sensitization of Refractory Murine Neuroblastoma to Checkpoint Inhibitor Therapy. Clinical Cancer Research. 2020;26(5):1152-61.

49. Cohen G, Chandran P, Lorsung RM, Tomlinson LE, Sundby M, Burks SR, et al. The Impact of Focused Ultrasound in Two Tumor Models: Temporal Alterations in the Natural History on Tumor Microenvironment and Immune Cell Response. Cancers. 2020;12(2):350.

50. Olive KP, Jacobetz MA, Davidson CJ, Gopinathan A, McIntyre D, Honess D, et al. Inhibition of Hedgehog signaling enhances delivery of chemotherapy in a mouse model of pancreatic cancer. Science. 2009;324(5933):1457-61.

51. Hassan S, Peluso J, Chalhoub S, Gillet YI, Benkirane-Jessel N, Rochel N, et al. Quercetin potentializes the respective cytotoxic activity of gemcitabine or doxorubicin on 3D culture of AsPC-1 or HepG2 cells, through the inhibition of HIF-1α and MDR1. PLoS One.

2020;15(10):e0240676.

52. Arnold RD, Slack JE, Straubinger RM. Quantification of Doxorubicin and metabolites in rat plasma and small volume tissue samples by liquid chromatography/electrospray tandem mass spectroscopy. Journal of Chromatography B. 2004;808(2):141-52.

초 록

목적: 췌장암 이종이식 모델에서 Doxorubicin을 탑재한 미세기포 집합체 (DMMC)와 집속초음파 평행 치료의 상호 증강 효과를 평가하고자 한다.

방법: 면역결핍 마우스에 CFPAC-1을 접종하여 췌장암 이종이식 모델을 만들었다. DMMC는 Doxorubicin을 탑재한 알부민 미세입자와 미세기포와의 결합을 통해 생성하였다. 집속초음파 치료를 위해 음향파워 80.5W, 반복 주기 (duty cycle) 5%를 적용하였다. 마우스는 총 5 군 (집단 별 개체 수=5) 으로 나누어 4mg/Kg Doxorubicin로 치료를 시행하였다. 5군은 1) 대조군, 2) Doxorubicin 단독, 3) Doxorubicin와 미세기포 혼합물에 집속초음파 치료, 4) Doxorubicin 탑재 알부민 미세입자와 미세기포 혼합물에 집속초음파 치료, 5) Doxorubicin 탑재 알부민 미세입자와 미세기포 집합체 (DMMC)에 집속초음파 치료로 이루어져 있다. 제 1단계에서는 DMMC와 집속초음파 치료의 효과를 확인하고자 하였다. 제 2단계에서는 혼합물과 집합체의 치료효과를 비교하고자 하였다. 병태생리학적 분석을 위해, 동일한 조건으로 반복 실험 하였고, 종양 apoptosis와 세포 내 Doxorubicin 흡수 양 을 형광분석을 통해 분석하였다. 통계분석에는 Bonferroni correction을 동반한 Kruskal-Wallis 검정과 Mann- Whitney 검정을 이용하였다.

결과: 제 1단계 실험에서 DMMC와 집속초음파 병행치료를 시행한 군에서 유의하게 작은 종양크기 및 가장 느린 종양 성장속도를 보여주었다. 제 2단계 실험에서는, 유일하게 DMMC와 집속초음파 병행치료를 시행한 군에서 대조군과 비교시 유의하게 낮은

성장속도를 보여주었다 (P=0.01). 병태생리학적 분석에서, DMMC와 집속초음파 병행치료를 시행한 군이 Doxorubicin 단독치료 혹은 Doxorubicin과 FUS 병행 치료군보다 높은 세포 내 Doxorubicin 흡수를 보였다 (Ps<.001). DMMC와 집속초음파 병행치료 군에서 종양세포 apoptosis 비율이 다른 실험군과 비교시 가장 높았다.

결론: DMMC와 집속초음파 병행치료는 췌장암 세포의 종양의 성장을 억제할 수 있는 것으로 사료되며, 이는 세포내의 높은 Doxorubicin 흡수에 기인한 것으로 보인다.

주 요 어 : 췌장암, 이종이식, 집속초음파, Doxorubicin, 미세기포
학 번 : 2016-36060